SimBuild
2024

Eleventh National Conference of IBPSA-USA
Denver, Colorado
May 21 – 23, 2024

Model Predictive Control for a Multi-modal Nocturnal Radiative Cooling System

Manuel Koch[1,2], Parantapa Sawant[2], Ralph Eismann[2] and Colin N. Jones[1]
[1]EPFL, Lausanne, Switzerland
[2]FHNW, Muttenz, Switzerland
{manuelpascal.koch, colin.jones}@epfl.ch
{manuel.koch, parantapa.sawant, ralph.eismann}@fhnw.ch

Abstract

In light of the rapidly increasing global energy demand for cooling, energy-efficient cooling methods should be investigated. We use chiller-assisted nocturnal radiative cooling with photovoltaic-thermal collectors to cool a single-family house in Central European summer climate. A model predictive controller chooses between active and passive operation to cool a radiant slab at night to stay below an upper zone temperature limit during the following day. This goal is achieved with a high energy-efficiency ratio, compared to a conventional cooling system, while keeping the computational demands of the model predictive controller low.

Introduction

The share of carbon-intensive fossil fuels in the global primary energy production is currently around 83 % (British Petroleum 2021). Considering the targets in carbon emission reduction declared by many countries (Bundesamt für Energie 2018; European Comission 2019), a stark increase in low-carbon power generation, and reduction in energy consumption can be expected in the coming decades. The work presented in this paper addresses both, albeit with a focus on the latter. The global energy consumption for cooling is rapidly increasing, driven by factors such as population growth, urbanization, and climate change (International Energy Agency 2018). It is therefore desirable to develop energy-efficient methods to meet this demand. One approach to do so is through nocturnal radiative cooling. The background temperature of outer space is approximately 3 K. On earth's surface, this is greatly attenuated by the atmosphere, but the effective sky temperature can still drop significantly below the ambient temperature, especially during clear nights. This phenomenon can often be observed on a cold morning, when the tops of cars are iced over, but not the sides. In ancient times, it was used to produce ice in the desert (Pomeroy 2018). For better illustration, Figure 1 shows the spectra of the sun's electromagnetic emission based on (NASA 2020), the atmospheric transmission[1] based on (American Society for Testing and Materials 2000), and the ideal black-body radiation at 25 °C based on Planck's law. We note that the band of high atmospheric transmission between the wavelengths of 8 µm to 12 µm roughly aligns with the peak of the black-body radiation. Thus, heat emitted at this temperature can penetrate the atmosphere into outer space well. The black-body radiation spectrum would be slightly shifted at different temperatures commonly found on earth's surface, but the point still holds. Furthermore, radiation spectra of real objects deviate from an ideal black-body, but for most common materials, it is a reasonable approximation.

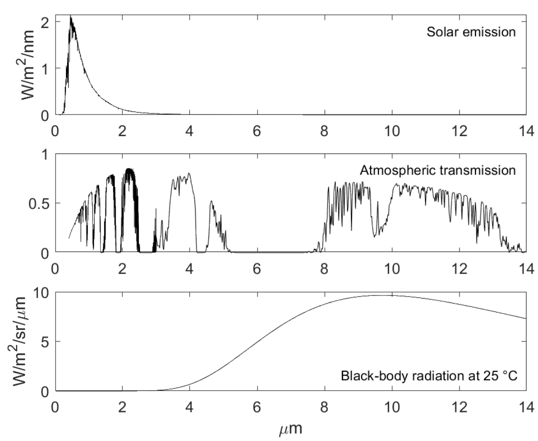

Figure 1: Spectra of solar emission, atmospheric transmission and ideal black-body radiation at 25 °C *at short and medium wavelengths*

Harnessing nocturnal radiative cooling for buildings requires a heat exchanging surface facing the sky, such as an unglazed solar-thermal collector. While the concept has been studied extensively (Fernandez et al. 2015; Hu et al. 2016; Lu et al. 2016; Zeyghami, Goswami, and Stefanakos 2018; Nwaji et al. 2019; Chen and Lu 2020), it is mostly used in parallel with a second cooling system, or to pre-cool water before entering a mechanical chiller. In

[1]This data set accounts for scattering at short wavelengths. Without it, the transmission of visible light would be around 90 %.

contrast, our approach uses a chiller to elevate the radiator temperature, if the weather conditions are insufficient for passive cooling. With this method, the active cooling mode still benefits from the sub-ambient sky temperature, boosting the energy efficiency ratio (EER) of the system. It also eliminates the need for an external fan unit and the noise that comes with it, which can be a significant advantage, considering the legal limits on nightly noise emissions in many residential areas (Bundesamt für Umwelt 2021). To the best of our knowledge, this method was previously only used by (Koch, Dott, and Eismann 2019), using a hand-tuned rule-based controller. We use data-driven model predictive control (MPC), leveraging readily available weather forecasts to predictively optimize the operation based on the specific cooling demand of the following day.

Furthermore, we use photovoltaic-thermal (PVT) collectors as radiators. This has the benefit of generating electricity, while also making the system suitable for solar-assisted heating, assuming a reversible chiller. We intend to investigate this in a more extensive follow-up study.

Our system configuration is shown on the left-hand side of Figure 2. The house can connect to the internal heat exchanger (HEX) or the chiller, which in turn connect to the PVT. The simpler system on the center-left is the reference system used in this study, detailed in the Methodology section. For comparison, the schematics on the center-right and right-hand side show the system configurations for nocturnal radiative cooling most commonly found in the literature. In the center-left system, the PVT pre-cools warm water from the building before entering the chiller, but it can also be bypassed if necessary. In the right-hand system, the PVT for radiative cooling and the conventional chiller are completely separated. We note that while the building-side hydraulics use water, a water-glycol mixture must be used in the external components to avoid frost damage. This is why the PVT does not connect to the building-side directly, but is connected to a heat exchanger instead. Table 1 summarizes the general advantages and disadvantages of the system configurations in Figure 2. Among the compared systems, ours is capable of active and passive heating and cooling, while running silently and requiring fewer components than the pre-cooling configuration. However, it is not capable of daytime cooling, giving particular importance to the application of predictive control.

Some studies take the concept of radiative cooling even further by performing daytime radiative cooling, using meta-materials designed to have a high emissivity in the band around 8 µm to 12 µm, where the atmosphere is usually transparent, while having a low emissivity (resp. absorptivity) in the visible range (Bijarniya, Sarkar, and Maiti 2020). However, due to the prototypical nature of these materials, we disregard them for this study, instead restricting our system design to commercially available components.

Since cooling demand overwhelmingly occurs during the day, nocturnal radiative cooling requires substantial thermal storage. Installing a dedicated water tank may be too expensive or not feasible due to a lack of space. To give an example, with a $\Delta T = 10\,\mathrm{K}$, the thermal storage capacity of $1\,\mathrm{m}^3$ of water is around 11.6 kWh. Thus, a large tank with a height of around 2 m and a diameter of around 1 m (including a 10 cm insulation layer) would barely suffice to cool a typical apartment unit in Central European summer conditions. The use of phase-change materials has been proposed many times, but never gained traction outside of academic studies, as concerns about the performance and cost of such materials have persisted (de Gracia and Cabeza 2015; Souayfane, Fardoun, and Biwole 2016; Faraj et al. 2020).

We address these concerns by using a radiant slab as a quasi-storage method. A concrete slab of 10 cm and $100\,\mathrm{m}^2$ with a $\Delta T = 4\,\mathrm{K}$ has a thermal storage capacity of around 20 kWh, depending on the exact properties of the concrete. The time constant of such a slab is likely to fall into a range of 7 h to 15 h, which is convenient, considering we want to shift the cooling load from day to night. Assuming that a building already has a radiant slab installed, this method can provide substantial storage capacity with no additional costs. The two main challenges with it are that, first, the cooling power is not controllable during the day. Instead, the slab must be cooled to an appropriate temperature during the night, based on the conditions of the following day and knowledge of the building's thermal properties, and is then left to absorb heat from the indoor air in a manner dictated by its physical properties. Second, avoiding both discomfort in the occupants during the coldest hours, and condensation of humid air puts a lower constraint on the permissible slab temperature and thus the cooling power and storage capacity. However, the general practicability of radiant slab cooling has been shown many times, (Tian and Love 2008; Hassan and Abdelaziz 2020), including a side-by-side comparison with a variable-air-volume system in an office building in the seasonally hot and humid climate of Hyderabad, India, which is the least favorable for this type of system, considering the challenges described above (Sastry and Rumsey 2014).

These constraints and long time constants make noctur-

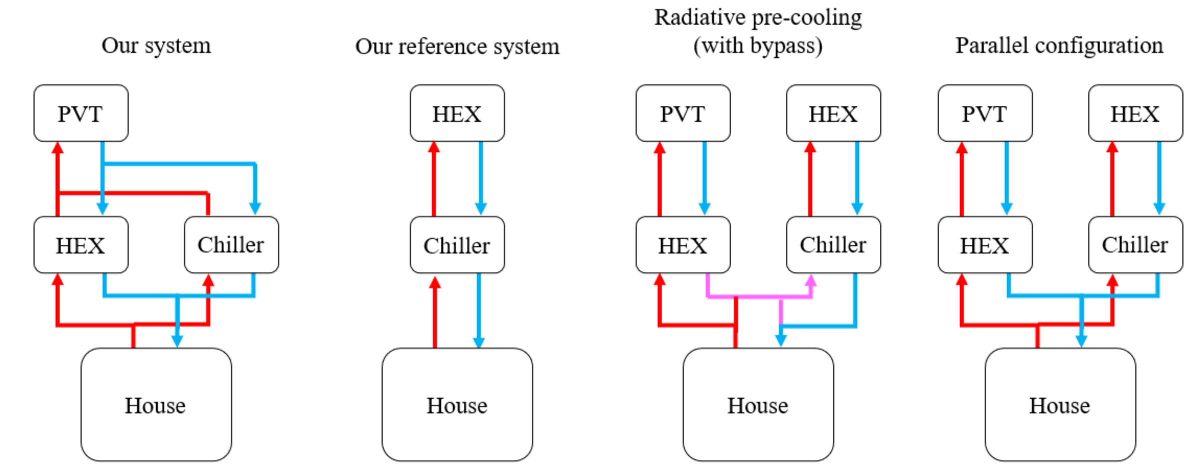

Figure 2: Simplified schematic of the system configuration on the left. Reference system on the center-left. Two alternative configurations commonly seen in the literature on the center-right and right.

Table 1: Comparison of different system configurations for nocturnal radiative cooling. ('+': Advantage/capable, '○': Neutral, '-': Disadvantage/not capable)

	Our system	**Reference**	**Pre-cooling**	**Parallel**
Silent (no external fan)	+	-	-	-
Fewer components	○	+	-	-
Daytime cooling	-	+	+	+
Nocturnal radiative cooling	+	-	+	+
Nocturnal radiation-assisted cooling	+	-	+	-
Solar-thermal heating	+	-	+	+
Solar-assisted heating (reversible chiller)	+	-	+	-

nal radiative cooling of a radiant slab an ideal application for MPC, whose effectiveness in buildings has already been proven many times (Serale et al. 2018; Drgoňa et al. 2020). If passive cooling is sufficient to reach the cooling target for the next day, there is no need to run the chiller, which consumes much more electricity. If running the chiller is necessary, it should preferably be done during the coldest hours of the night, when the EER is at its highest. Since the upfront engineering costs of building a sufficiently accurate model have been identified as a major roadblock for the commercialization of MPC in buildings (Killian and Kozek 2016; Hilliard, Kavgic, and Swan 2016), we rely on measurement data and system identification to obtain a model. To keep the computational requirements and thus the hardware costs low as well, we avoid highly computationally intensive modeling methods such as Gaussian processes or neural networks for the time being, despite their potential to yield more accurate models (Maddalena, Lian, and Jones 2020; Di Natale et al. 2022b).

In this paper, we conduct a simulation study on nocturnal radiative cooling of a building using MPC. Despite the system being designed for heating and cooling, we currently restrict our scope to cooling, which is the more novel aspect, and more likely to be a limiting factor for such a system, compared to heating, which is the intended purpose of PVT collectors. The following chapters cover the details of the simulation model, the system identification, the MPC, the reference system for the performance evaluation, the numerical results, as well as a discussion of and conclusions drawn from these results.

Methodology

Physical model

We modeled the single-zone single-family house shown in Figure 3 based on (Dott et al. 2014b) as a Matlab ordinary differential function, executing it with *ode23t*, which is a stiff solver without numerical damping, well-suited to simulating physical systems that have both fast and slow time constants. The building has two storeys, a usable area of 140 m^2 with an underfloor radiant slab, and is representative of newly built Central European houses, having a nominal heating energy consumption of 45 kWh/m^2/yr.

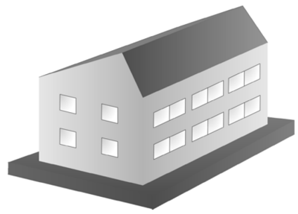

Figure 3: Drawing of the building model from a north-east angle (Dott et al. 2014b)

Each of the two floors has an area of 70 m^2, is modeled as five thermal nodes, and has an 8 cm thick concrete radiant slab under the wooden flooring. The external brick walls have an area of 221.1 m^2 and are modeled as four nodes. The roof has a total area of 84.1 m^2 and is modeled as four nodes as well. The furniture is modeled as 200 m^2 of clinker[2] wall, represented by one node. The inside air totals 389.45 m^3 and is lumped into one node. The convective heat transfer rates on the horizontal surfaces are modeled based on (Glück 2007), while the convective heat transfers on the vertical and outer surfaces are linearized to constant values based on (Glück 2007) and (International Organization for Standardization 2017a). There are windows on each façade with a total area of 23 m^2. Their heat transfer coefficient is 1.5 W/m^2/K and the G value is 0.622. The solar gains are introduced into the top-layers of the two floors and the external walls, with the former getting 40 % each and the latter getting 20 %. The insulation layers measure 12 cm at the external walls, and 16 cm at the roof and under the ground floor. The ground temperature is modeled as a constant 15 °C.

While the building geometry and materials follow the source closely, we made several adjustments to the heating, ventilation and air conditioning (HVAC) components for the purpose of this study. We added a mechanical ventilation with a heat recovery of 60 %, which should improve the energy efficiency beyond the nominal value. Each façade has an independently controlled shading system, limiting the perpendicular solar radiation to 180 W/m^2, measured outside of the windows. This value is intentionally set rather low, since the overall goal is to lower the energy consumption for cooling.

[2]Partially-vitrified fired clay bricks

The internal brine-water heat exchanger is modeled based on the number of transfer units (NTU) method. The combined power of the circulation pumps is 100 W. The external air-brine heat exchanger of the reference system is modeled as one thermal node and its fan has a power of 200 W.

The PVT collectors have lamella heat exchangers mounted on their backsides to increase convective heat transfer, are modeled as one thermal node, and cover an area of 58.8 m^2 on the south-facing side of the roof. This orientation is not ideal for cooling and is motivated by an intended dual-use for heating. The model parameters $\eta_{o,b}$, κ, K_d and a_1 to a_8 of equation (1) were determined experimentally according to *ISO 9806:2017* (International Organization for Standardization 2017b) and are listed in Table 2.

$$\begin{aligned}\dot{q} =&\eta_{o,b}K_b(\alpha)I_{col,dir} + \eta_{o,b}K_d I_{col,dif} - a_1(T_{col} - T_{amb}) \\ &- a_2(T_{col} - T_{amb})^2 - a_3 v'(T_{col} - T_{amb}) - a_5\frac{dT_{col}}{dt} \\ &- a_6 v' I_{col} - a_7 v' \sigma(T_{sky}^4 - T_{col}^4) - a_8(T_{col} - T_{amb})^4\end{aligned} \quad (1)$$

With $\eta_{o,b}$ the zero loss efficiency, $K_b(\alpha) = 1 - tan^{\kappa}(\alpha/2)$ the angular dependence for direct solar radiation based on the Ambrosetti function, α the incident angle, $I_{col,dir}$ the direct solar radiation on the collector, K_d the angular dependence for diffuse radiation, $I_{col,dif}$ the diffuse solar radiation on the collector, T_{col} the mean collector temperature, T_{amb} the ambient temperature, $v' = v_{wind} - 3\,\mathrm{m/s}$ the modified wind speed, T_{sky} the radiative sky temperature, σ the Stefan-Boltzmann constant, and I_{col} the total solar radiation on the collector.

We assume a photovoltaic conversion efficiency of 19 % and 5 % inverter losses. Since this is power that is extracted from the system, and the experimental parameters were determined without electricity generation, we adjust the calculation of the thermal power in equation (1) by subtracting 19 % from the solar radiation on the collector. Since this happens during the day, its impact on nocturnal cooling is marginal.

The chiller for active cooling has an electrical power of 800 W and a nominal EER of 3.0 at a temperature lift of 35 K. The EER is modeled as the cropped exponential function (2) of the temperature lift ΔT. The calculation of the EER as an exponential function of the temperature lift is taken from (Gasser et al. 2017), albeit with adjusted numerical values to be more representative of typical chillers using scroll compressors. Comparable

Table 2: Experimentally determined model parameters for PVT collectors

Parameter	Unit	Value
$\eta_{o,b}$		0.402
κ		4.363
K_d		0.887
a_1	$W/m^2/K$	24.988
a_2	$W/m^2/K^2$	0.15
a_3	$Ws/m^3/K$	4.036
a_4		0.058
a_5	$Ws/m^2/K$	6819.4
a_6	s/m	0.032
a_7	s/m	0.083
a_8	$W/m^2/K$	0

efficiency values for very low-lift regimes are reported in (Dott et al. 2014a). The same chiller parameters are used for the nocturnal cooling and the conventional reference system.

$$EER = max(7,\ 7e^{-0.0242\ \Delta T}) \tag{2}$$

Weather data and internal gains

We use the EnergyPlus weather data set for Strasbourg, France (EnergyPlus 2023). The city of Strasbourg is also used to represent Central European climate in the design of the building model in (Dott et al. 2014b). The sky temperature is calculated using the default method in the LBNL Modelica Buildings Library, version 8.0.0, based on the dry bulb temperature, the dew point and the cloud cover (Lawrence Berkeley National Laboratory 2023). A perfect weather forecast with a 24 h horizon is used. While a realistic weather forecast would have been preferable, no such data was available to us at the time. We intend to address this issue in the previously mentioned more extensive follow-up study. However, considering the quality of modern weather forecasts (Meteoblue 2023), we currently believe that this only has a moderate impact on the performance.

Figure 4 shows the daily internal gains profile. It is based on the assumption of a four-person family (two adults, two children). There is a constant 50 W baseline from various household appliances. Each present occupant adds 60 W at night and 100 W during the day, to account for the use of personal devices. In the late evening hours, there is an additional 50 W for lighting. We assume some use of cooking appliances in the morning (100 W) and at noon (200 W), when two occupants are present. Since we simulate the hottest part of the year with long daylight hours, we assume that the use of lighting and cooking appliances, as well as the occupancy during the early evening hours, is below the annual average. This results in a daily average of 252.5 W. While this may seem relatively low, we note here that we assume the use of devices with high energy-efficiency, in accordance with European energy policies (European Comission 2021), including induction cooktops, which have a thermal efficiency, i.e. the share of the power that is transferred into the food and not into the air, of around 90 %, compared to 75 % for conventional electric systems and 40 % for gas (Sweeney et al. 2014).

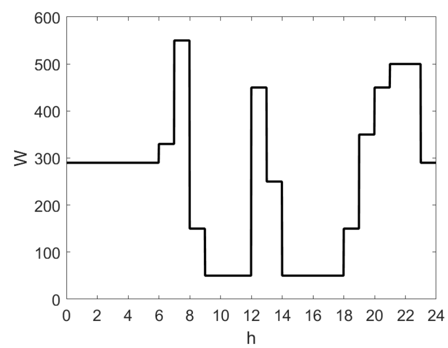

Figure 4: Daily internal gains profile

System identification

A model $\theta \in \mathbb{R}^{2\times 15}$ predicting $y = \begin{pmatrix} T_{zone} & T_{slab} \end{pmatrix}^\top$ is identified, expressing the thermal state of the building through the zone and slab temperatures. Simple models with one or two states have been shown to perform similarly to more complex ones for the identification of building thermodynamics (Fux et al. 2014). The time step is 3600 s, which we found to be a reasonable value, considering the heavy construction style of the building with a radiant slab. We assume that the slab temperature is known. This can be realized by embedding temperature sensors in it, or by maintaining a small flow through the slab's piping and measuring the water temperature at the outlet. The input φ_k at time step k in equation (3) for the prediction in equation (4) is comprised of the current state of the building y_k, the ambient temperature $T_{amb,k}$ and the global horizontal solar radiation $I_{glo,k}$ as external disturbances, and a number of control terms for the active and passive cooling.

$$\varphi_k = [T_{zone},\ T_{slab},\ T_{amb},\ I_{glo},\ T_{slab}\delta_{hex},\ T_{amb}\delta_{hex},\ T_{sky}\delta_{hex},\ v_{wind}\delta_{hex},\ \delta_{hex},\ T_{slab}\delta_{ch},\ T_{amb}\delta_{ch},\ T_{sky}\delta_{ch},\ v_{wind}\delta_{ch},\ \delta_{ch},\ 1]_k^\top \quad (3)$$

$$y_{k+1} = \theta\varphi_k \quad (4)$$

These terms are derived from the general physical model of a solar-thermal collector in equation (5), which differs from the parametrization used in *ISO 9806:2017*. We use the binary control variables δ_{hex} for the passive heat exchanger and δ_{ch} for the active chiller as linear inputs. This is augmented by four bilinear terms for each, multiplied by T_{slab} (i.e. the sink temperature for the cooling system), T_{amb}, the sky temperature T_{sky} and the wind speed v_{wind}; as well as a constant offset term, which we found to improve the model accuracy. We attribute this to the fact that we normalize each recorded data channel individually, before some of them are combined into bilinear terms, which are then no longer unbiased.

$$C_{col}\dot{T}_{col} = c_b\dot{m}(T_{in} - T_{col}) + H_{col}(v_{wind})(T_{amb} - T_{col}) \\ A_{col}\varepsilon_{col}I_{col} + \sigma\varepsilon_{IR}A_{col}(T_{sky}^4 - T_{col}^4) \quad (5)$$

With C_{col} the thermal capacity of the collectors, T_{col} its temperature, $\dot{m}$ the mass flow through it, T_{in} its supply temperature, $H_{col}(v_{wind})$ its wind speed dependent convective heat transfer, A_{col} its area, ε_{col} its overall radiative emissivity, I_{col} the perpendicular solar radiation, σ the Stefan-Boltzmann constant, and ε_{IR} its infrared emissivity.

Some of these terms may be highly correlated (e.g. T_{amb} and T_{sky}), which can be a source of problems in system identification. We therefore impose physical constraints on the parameters for the identification, summarized in Table 3. Similar methods have been used successfully by (Bünning et al. 2022) and (Di Natale et al. 2022a). In the absence of external influences, T_{zone} and T_{slab} should converge, without oscillations or autonomous increases. The corresponding parameters are thus limited to $(0,1)$. Furthermore, the sum of the auto-regressive parameters for each output are restricted to $\theta_{zone\to zone} + \theta_{slab\to zone} \leq 1$ and $\theta_{zone\to slab} + \theta_{slab\to slab} \leq 1$. Higher T_{amb} and I_{glo} should have a positive effect on the temperatures in the building. Regarding the control variables for both the heat exchanger and chiller, a higher T_{slab} should increase the collector temperature and heat dissipation, and thus have a negative effect on the building temperatures. A higher v_{wind} increases the convection at the collectors, having the same effect. A higher T_{amb} and T_{sky} hinder the cooling, thus have a positive effect on the building temperatures. The linear weights for δ_{hex} and δ_{hp} are negative, since it is a cooling system. These constraints on θ form the set Θ. The Frobenius norm of the one-step prediction across the identification data set, which is collected during the whole month of July, is then minimized according to equation (6), with $Y = \begin{pmatrix} y_2 & \dots & y_M \end{pmatrix} \in \mathbb{R}^{2\times M-1}$, $\Phi = \begin{pmatrix} \varphi_1 & \dots & \varphi_{M-1} \end{pmatrix} \in \mathbb{R}^{15\times M-1}$ and M the number of samples in the identification data set. For each night of the identificatin period, the HVAC system is either doing nothing, cooling actively or cooling passively in a randomized order, but stops if the slab temperature drops to 21 °C.

Table 3: Physical constraints on the model parameters. Positive, negative, in range or unconstrained.

Input/Output	T_{zone}	T_{slab}
T_{zone}	$(0,1)$	$(0,1)$
T_{slab}	$(0,1)$	$(0,1)$
T_{amb}	$+$	$+$
I_{glo}	$+$	$+$
$T_{slab}\delta_{hex}$	$-$	$-$
$T_{amb}\delta_{hex}$	$+$	$+$
$T_{sky}\delta_{hex}$	$+$	$+$
$v_{wind}\delta_{hex}$	$-$	$-$
δ_{hex}	$-$	$-$
$T_{slab}\delta_{hp}$	$-$	$-$
$T_{amb}\delta_{hp}$	$+$	$+$
$T_{sky}\delta_{hp}$	$+$	$+$
$v_{wind}\delta_{hp}$	$-$	$-$
δ_{hp}	$-$	$-$
Offset term		

$$\min_{\theta} \|Y - \theta\Phi\|_F^2 \quad (6) \\ s.t. \\ \theta \in \Theta$$

Model Predictive Control

The MPC in equation (7) is implemented in Gurobi, version 10.0 (Gurobi 2023), and seeks to minimize the electric energy consumed to run the cooling system while respecting the temperature constraints on the zone and the slab. Combining the power of the chiller and circulation pumps, we obtain the weights $P_{el,hex} = 100\,\mathrm{W}$

and $P_{el,ch} = 900\,\mathrm{W}$. y is the state, as defined above. $u = \begin{pmatrix}\delta_{hex} & \delta_{ch}\end{pmatrix}^\top$ is the control input for the internal heat exchanger and the mechanical chiller. $w = \begin{pmatrix}T_{amb} & I_{glo}\end{pmatrix}^\top$ is the disturbance input, containing the ambient temperature and the global horizontal solar radiation. All normalization is omitted in the equations for the sake of legibility. The current state, the most recent control input and the future weather are known (7b). Equation (7c) is an abbreviation of the system dynamics in equation (3). Equations (7d) and (7e) are the input and output constraints. The system can only be activated at night (7f). Active and passive cooling cannot run simultaneously (7g), and can each only be activated for one continuous phase per night (7h,7i), including the current time step, hence the sum begins at time step $j = -1$. This is a mixed-integer linear problem, which are known to be computationally expensive.

$$\min_{u,y} \sum_{k=0}^{N-1} (P_{el,hex}\delta_{hex,k} + P_{el,ch}\delta_{ch,k}) \tag{7a}$$

$$s.t.$$

$$y_0, u_{-1}, w_{[0:N-1]} \text{ known} \tag{7b}$$

$$y_{k+1} = f(y_k, u_k, w_k) \tag{7c}$$

$$\begin{pmatrix}21.5\,^\circ\mathrm{C} \\ 20\,^\circ\mathrm{C}\end{pmatrix} \leq y \leq \begin{pmatrix}24.5\,^\circ\mathrm{C} \\ \infty\end{pmatrix} \tag{7d}$$

$$u \in \{0,1\}^2 \tag{7e}$$

$$u_k = 0 \text{ if } I_{glo,k} > 3\,\mathrm{W/m^2} \tag{7f}$$

$$\delta_{hex,k} + \delta_{ch,k} \leq 1 \tag{7g}$$

$$\sum_{j=-1}^{N-1} |\delta_{hex,j+1} - \delta_{hex,j}| \leq 2 \tag{7h}$$

$$\sum_{j=-1}^{N-1} |\delta_{ch,j+1} - \delta_{ch,j}| \leq 2 \tag{7i}$$

$$\forall k \in \{0, \ldots, N-1\}$$

The zone temperature is restricted to $T_{zone} \in [21\,^\circ\mathrm{C}, 25\,^\circ\mathrm{C}]$, which complies with the recommendations of *SIA 180:2014* (Schweizerischer Ingenieur- und Architektenverein 2014) for Summer climate in Switzerland. While these temperatures may seem to be comparatively high, we note that this standard aims to strike a balance between occupant comfort and energy efficiency, and assumes that light clothing is worn inside. The slab temperature is constrained to $T_{slab} \geq 20\,^\circ\mathrm{C}$ to avoid condensation. The optimization horizon is $N = 24$, corresponding to 24 h. Based on the observed accuracy of the 24 h-ahead prediction with the identified model, the actual constraints on the zone temperature for the optimization in equation (7d) are tightened by 0.5 K on each side. Since constraint satisfaction cannot be guaranteed, they are implemented as soft constraints. We note that for the evaluation of the constraint violations in the results section, the unaltered constraints stated above are used.

Reference system and controller

As indicated above, the reference system uses the same chiller as the nocturnal cooling, but with an external air-brine heat exchanger unit instead of the PVT collectors. A binary rule-based hysteresis controller with the switching temperatures 24 °C and 25 °C is used. The upper temperature corresponds to the comfort constraint for the MPC. Choosing the width of the hysteresis is a trade-off between energy efficiency and mechanical wear: A narrower band would improve the efficiency by elevating the average zone temperature by around half of its width, but would require more frequent on-off cycles, which strains the chiller and valves. A hysteresis of 1 K is a common choice, and is shown to work well in the following section.

Results

Two simulations covering the month of August are conducted: One with the predictive nocturnal radiative cooling system, and one with the conventional reference system. The results in Table 4 show a 34 % reduction in electricity consumption with the nocturnal cooling while supplying 6.2 % more thermal cooling energy, corresponding to a 62 % increase of the EER. This can be attributed to three factors: When cooling actively at night, the chiller benefits from the lower ambient (i.e. sink) temperature, compared to the rule-based system, which mostly runs during the hotter day-time hours. Furthermore, the PVT collectors have no electricity-consuming fans, unlike the external heat exchanger. Lastly, 27 % of the nocturnal cooling is supplied passively. Thanks to its very high EER, which is in the nature of passive cooling, this is enough to substantially improve the total efficiency. The increase in delivered thermal energy with the nocturnal cooling is unsurprising, since the cooling happens around 12 h ahead of the demand, which leads to some losses. All constraint violations with both the nocturnal cooling and the reference system are negligible, none of them exceeding a few Kelvin-hours over 31 days. Furthermore, the PVT collectors generate 2.25 MWh of electricity during the simulation period.

Figure 5 shows the whole simulation with nocturnal cooling. The zone temperature mostly stays between 23 °C and 25 °C. One 2 K oscillation of the zone temperature per day is a slow rate of change that does not cause thermal discomfort in the occupants. The MPC occasionally shows undesirable fast-switching behavior, caused by the inaccuracies of the prediction model, like on days 217 and 218, where the controller quickly switches from active cooling, to off, to passive cooling. Other than that, the mixed-integer optimization problem is solved quickly and reliably, which is important for deployment on cheap low-power hardware. The time required for an individual solution mostly stayed between 0.01 s and 0.3 s, averaging around 0.1 s, on a four-core *Intel Core i7-8665U* processor. The close-up in Figure 6 shows five days of operation, with one night of active cooling, one night of passive cooling and three days of mixed cooling, including the aforementioned days with undesirable fast-switching, while respecting the temperature constraints at all times. The order of active and passive in the case of mixed cooling depends on the state of the building and the weather. In general, passive cooling is more dependent on favorable conditions, ideally a high slab temperature with cool, clear and windy weather, and should be scheduled accordingly. Since the passive cooling is also less powerful than the active cooling, its identification and thus prediction may be less accurate, which may lead to less optimal scheduling.

For comparison, we also show the results of the reference simulation with the conventional rule-based cooling, including the weather conditions, in Figure 7. Cooling on demand during the day allows to keep the zone temperature in a narrower band, mostly between 24 °C and 25 °C, which comes at the cost of a lower EER however.

Table 4: Energy use for cooling during August with the reference system (top), and the nocturnal cooling (bottom), split into its active and passive components.

	Electrical kWh	**Thermal** kWh	**EER**
Reference	125.4	591.3	4.7
Passive	5.1	170.6	33.4
Active	77.4	457.2	5.9
Total	82.5	627.8	7.6

Discussion

While cooling with a very high efficiency is achieved, the practical drawbacks of nocturnal radiative cooling remain: Namely the lack of temperature control during the day which, in combination with comfort constraints, significantly limits the cooling power and capacity, as well as the large surface area required by the collectors to dissipate the heat. We believe that the most promising path to commercial viability is the synergistic extension from just cooling to a multi-energy system. An extended follow-up study using the PVT collectors for day-time heating as well as nocturnal cooling is planned.

The lack of controllability during the day could be addressed by adding a storage tank for cold water to the system, or by using conventional air conditioning as a back-up. However, since this would add to the system costs, it is preferable to make the nocturnal cooling of the radiant slab work by itself. We thus utilized neither of these options, in order to focus on feasibility of doing so.

We further note that our case study in Central European climate is far from the ideal setting for such a system. A hotter, more arid climate with lower sky temperatures at night would be advantageous for nocturnal radiative cooling, as well as solar heat and electricity generation during the day. Such conditions happen to be found in many of the developing regions of the world where the energy demand for cooling is growing most rapidly (International Energy Agency 2018).

Moreover, the limited accuracy of the current model (i.e. system identification method) necessitated an additional tightening of the temperature constraints. A more accurate model would allow a reduction of these safety margins, which would improve the energy efficiency by reducing excessive cooling. Therefore, alternative model structures and identification procedures should be investigated in the future. A key question will be the trade-off between improved prediction accuracy and thus energy efficiency on one hand, and higher hardware costs to run a more complex model on the other. A secondary benefit of an improved model might also be a smoother operation with fewer on-off cycles, which would reduce the wear on the mechanical components.

Conclusion

A PVT-based nocturnal radiative cooling system with a data-driven MPC for a single-family house is evaluated in a simulation. Compared to a conventional chiller system with rule-based control, substantial energy savings of around 34 % are achieved, without sacrificing thermal comfort. This is a promising basis for further development of the system toward dual-use for heating and cooling. An MPC formulation is given that solves quickly and reliably enough to be suitable for deployment in the field with reasonable hardware costs. However, some

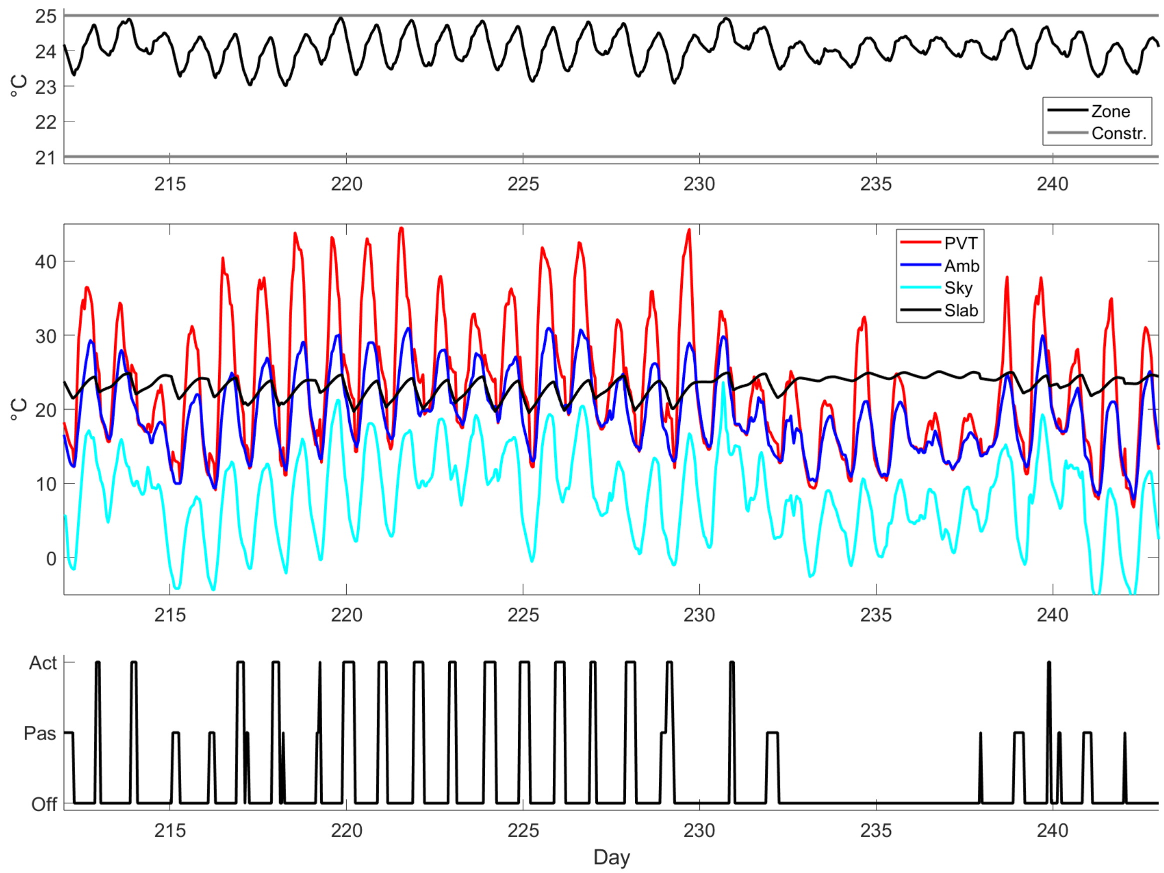

Figure 5: Nocturnal cooling with MPC. Top: Zone temperature and constraints. Middle: PVT collectors, ambient, sky and slab temperatures. Bottom: Active or passive cooling.

improvements in the system identification are desired to make the system run more smoothly, with fewer on-off cycles.

References

American Society for Testing and Materials. 2000. Standard Extraterrestrial Spectrum Reference E-490-00. https://www.nrel.gov/grid/solar-resource/spectra-astm-e490.html.

Bijarniya, Jay Prakash, Jahar Sarkar, and Pralay Maiti. 2020. "Review on Passive Daytime Radiative Cooling: Fundamentals, Recent Researches, Challenges and Opportunities." *Renewable and Sustainable Energy Reviews* 133 (November): 110263.

British Petroleum. 2021. Statistical Review of World Energy (2021). https://www.bp.com/content/dam/bp/business-sites/en/global/corporate/pdfs/energy-economics/statistical-review/bp-stats-review-2021-full-report.pdf.

Bundesamt für Energie. 2018. Energiestrategie 2050. https://www.bfe.admin.ch/bfe/de/home/politik/energiestrategie-2050.html.

Bundesamt für Umwelt. 2021. Belastungsgrenzwerte Für Lärm. https://www.bafu.admin.ch/bafu/de/home/themen/laerm/fachinformationen/laermbelastung/grenzwerte-fuer-laerm/belastungsgrenzwerte-fuer-laerm.html.

Bünning, Felix, Benjamin Huber, Adrian Schalbetter, Ahmed Aboudonia, Mathias Hudoba de Badyn, Philipp Heer, Roy S. Smith, and John Lygeros. 2022. "Physics-Informed Linear Regression Is Competitive with Two Machine Learning Methods in Residential Building MPC." *Applied Energy* 310 (March): 118491.

Chen, Jianheng, and Lin Lu. 2020. "Development of

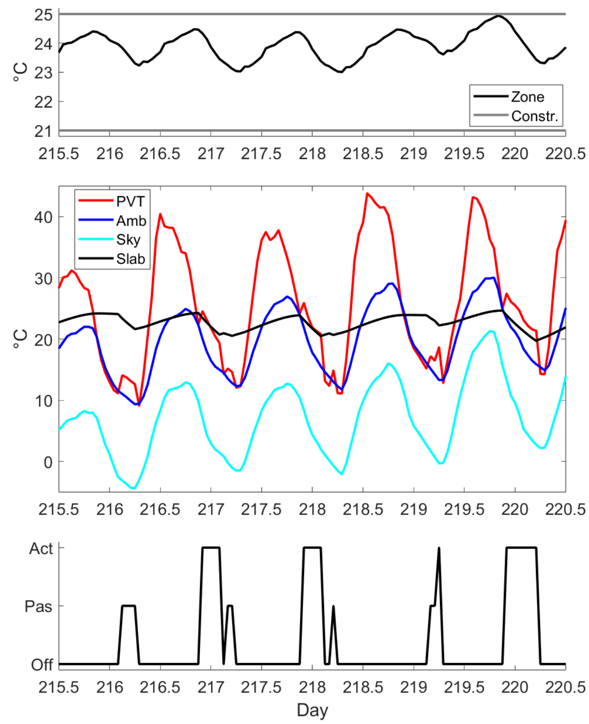

Figure 6: Close-up of Figure 5: Nocturnal cooling with MPC

Radiative Cooling and Its Integration with Buildings: A Comprehensive Review.” *Solar Energy* 212 (December): 125–151.

de Gracia, Alvaro, and Luisa F. Cabeza. 2015. “Phase Change Materials and Thermal Energy Storage for Buildings.” *Energy and Buildings* 103 (September): 414–419.

Di Natale, L., B. Svetozarevic, P. Heer, and C. N. Jones. 2022a. “Physically Consistent Neural Networks for Building Thermal Modeling: Theory and Analysis.” *Applied Energy* 325 (November): 119806.

Di Natale, Loris, Yingzhao Lian, Emilio T. Maddalena, Jicheng Shi, and Colin N. Jones. 2022b, December. “Lessons Learned from Data-Driven Building Control Experiments: Contrasting Gaussian Process-based MPC, Bilevel DeePC, and Deep Reinforcement Learning.” *2022 IEEE 61st Conference on Decision and Control (CDC)*. 1111–1117.

Dott, Ralf, Thomas Afjei, Andreas Genkinger, Antoine Dalibard, Daniel Carbonell, Ricard Consul, Andreas Heinz, Michel Haller, Andreas Witzig, Jorge Facão, Fabian Ochs, and Peter Pärisch. 2014a, October. *Models of Sub-Components and Validation for the IEA SHC Task 44 / HPP Annex 38 Part C: Heat Pump Models*.

Dott, Ralf, Michel Haller, Jörn Ruschenburg, Fabian Ochs, and Jacques Bony. 2014b, October. *The Reference Framework for System Simulations of the IEA SHC Task 44 / HPP Annex 38 Part B: Buildings and Space Heat Load*.

Drgoňa, Ján, Javier Arroyo, Iago Cupeiro Figueroa, David Blum, Krzysztof Arendt, Donghun Kim, Enric Perarnau Ollé, Juraj Oravec, Michael Wetter, Draguna L. Vrabie, and Lieve Helsen. 2020. “All You Need to Know about Model Predictive Control for Buildings.” *Annual Reviews in Control*, September.

EnergyPlus. 2023. Weather Data Strasbourg. Accessed June 5, 2023. `https://energyplus.net/weather-location/europe\_wmo\_region\_6/FRA/FRA\_Strasbourg.071900\_IWEC`.

European Comission. 2019. A European Green Deal. `https://commission.europa.eu/strategy-and-policy/priorities-2019-2024/european-green-deal\_en`.

European Comission. 2021. New EU energy labels applicable from 1 March 2021. `https://ec.europa.eu/commission/presscorner/detail/en/ip\_21\_818`.

Faraj, Khaireldin, Mahmoud Khaled, Jalal Faraj, Farouk Hachem, and Cathy Castelain. 2020. “Phase Change Material Thermal Energy Storage Systems for Cooling Applications in Buildings: A Review.” *Renewable and Sustainable Energy Reviews* 119 (March): 109579.

Fernandez, Nicholas, Weimin Wang, Kyle J. Alvine, and Srinivas Katipamula. 2015, November. “Energy Savings Potential of Radiative Cooling Technologies.” Technical Report PNNL-24904, Pacific Northwest National Lab. (PNNL), Richland, WA (United States).

Fux, Samuel F., Araz Ashouri, Michael J. Benz, and Lino Guzzella. 2014. “EKF Based Self-Adaptive Thermal Model for a Passive House.” *Energy and Buildings* 68 (January): 811–817.

Gasser, Lukas, Stefan Flück, Mirko Kleingries, Christoph Meier, Marc Bätschmann, and Beat Wellig. 2017, May. “High Efficiency Heat Pumps for Low Temperature Lift Applications.” *12th IEA Heat Pump Conference*. Rotterdam.

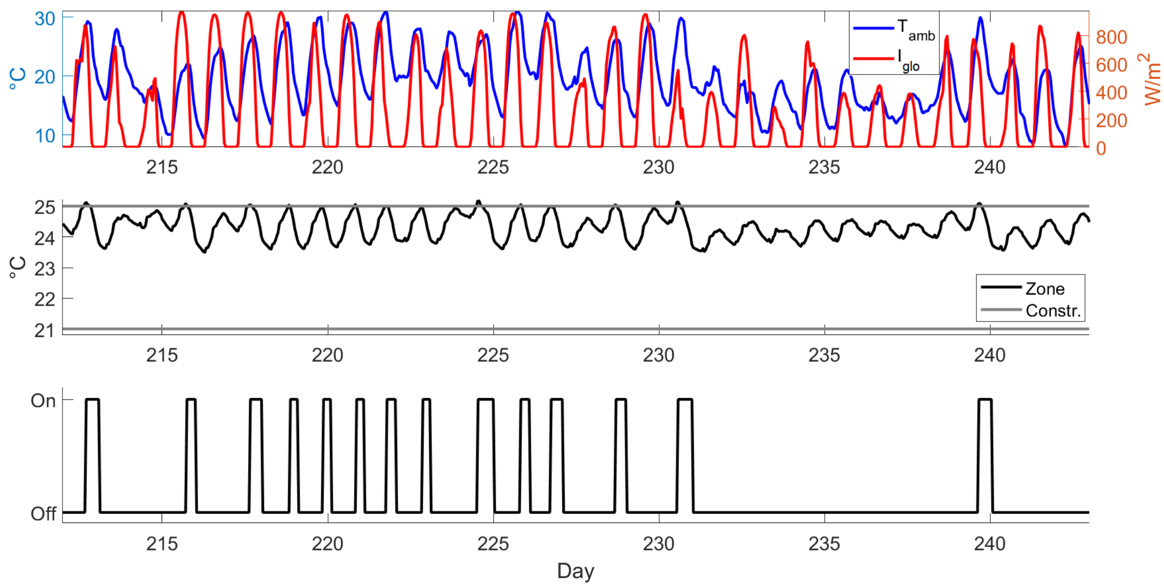

Figure 7: Reference system. Top: Ambient temperature and global horizontal radiation. Middle: Zone temperature and constraints. Bottom: Control.

Glück, Bernd. 2007. "Wärmeübergangskoeffizienten an Thermisch Aktiven Bauteiloberflächen Und Der Übergang Zu Basiskennlinien Für Die Wärmestromdichte." *Gesundheits-Ingenieur* 128 (1): 1–10.

Gurobi. 2023. The Leader in Decision Intelligence Technology. Accessed June 5, 2023. `https://www.gurobi.com/`.

Hassan, Muhammed A., and Omar Abdelaziz. 2020. "Best Practices and Recent Advances in Hydronic Radiant Cooling Systems – Part II: Simulation, Control, and Integration." *Energy and Buildings* 224 (October): 110263.

Hilliard, Trent, Miroslava Kavgic, and Lukas Swan. 2016. "Model Predictive Control for Commercial Buildings: Trends and Opportunities." *Advances in Building Energy Research* 10 (2): 172–190 (July).

Hu, Mingke, Gang Pei, Qiliang Wang, Jing Li, Yunyun Wang, and Jie Ji. 2016. "Field Test and Preliminary Analysis of a Combined Diurnal Solar Heating and Nocturnal Radiative Cooling System." *Applied Energy* 179 (October): 899–908.

International Energy Agency. 2018, May. The Future of Cooling – Opportunities for Energy-Efficient Air Conditioning. `https://www.iea.org/reports/the-future-of-cooling`.

International Organization for Standardization. 2017a. ISO 6946:2017: Building components and building elements - Thermal resistance and thermal transmittance - Calculation methods.

International Organization for Standardization. 2017b. ISO 9806:2017: Solar-energy - Solar thermal collectors - Test methods.

Killian, M., and M. Kozek. 2016. "Ten Questions Concerning Model Predictive Control for Energy Efficient Buildings." *Building and Environment* 105 (August): 403–412.

Koch, Manuel, Ralf Dott, and Ralph Eismann. 2019. "CoolShift – Cooling of Buildings by Chiller-Assisted Nocturnal Radiation and Convection." *Journal of Physics: Conference Series* 1343 (1): 012101 (November).

Lawrence Berkeley National Laboratory. 2023. Modelica Buildings Library: Buildings.BoundaryConditions.SkyTemperature. Accessed June 5, 2023. `https://simulationresearch.lbl.gov/modelica/releases/v8.0.0/help/Buildings\_BoundaryConditions\_SkyTemperature.html\#Buildings.BoundaryConditions.SkyTemperature`.

Lu, Xing, Peng Xu, Huilong Wang, Tao Yang, and Jin Hou. 2016. "Cooling Potential and Applications Prospects of Passive Radiative Cooling in Buildings: The Current State-of-the-Art." *Renewable and Sustainable Energy Reviews* 65 (November): 1079–1097.

Maddalena, Emilio T., Yingzhao Lian, and Colin N. Jones. 2020. "Data-Driven Methods for Building Control — A Review and Promising Future Directions." *Control Engineering Practice* 95 (February): 104211.

Meteoblue. 2023. Weather Data Accuracy. Accessed May 8, 2023. https://content.meteoblue.com/en/research-education/weather-data-accuracy/.

NASA. 2020, August. The Intervening Atmosphere: Tracing the Provenance of a Favorite Landsat Infographic. https://landsat.gsfc.nasa.gov/article/the-intervening-atmosphere-tracing-the-provenance-of-a-favorite-landsat-infographic/.

Nwaji, G. N., C. A. Okoronkwo, N. V. Ogueke, and E. E. Anyanwu. 2019. "Hybrid Solar Water Heating/Nocturnal Radiation Cooling System I: A Review of the Progress, Prospects and Challenges." *Energy and Buildings* 198 (September): 412–430.

Pomeroy, Ross. 2018, July. How People Created Ice in the Desert 2,000 Years Ago. https://www.realclearscience.com/blog/2018/07/09/how_people_created_ice_in_the_desert_2000_years_ago.html.

Sastry, G., and Peter Rumsey. 2014. "VAV vs. radiant: Side-by-side comparison." *ASHRAE J.* 56 (05): 16–24.

Schweizerischer Ingenieur- und Architektenverein. 2014. Norm SIA 180:2014: Wärmeschutz, Feuchteschutz und Raumklima in Gebäuden.

Serale, Gianluca, Massimo Fiorentini, Alfonso Capozzoli, Daniele Bernardini, and Alberto Bemporad. 2018. "Model Predictive Control (MPC) for Enhancing Building and HVAC System Energy Efficiency: Problem Formulation, Applications and Opportunities." *Energies* 11 (3): 631 (March).

Souayfane, Farah, Farouk Fardoun, and Pascal-Henry Biwole. 2016. "Phase Change Materials (PCM) for Cooling Applications in Buildings: A Review." *Energy and Buildings* 129 (October): 396–431.

Sweeney, Micah, Jeff Dols, Brian Fortenbery, and Frank Sharp. 2014. Induction Cooking Technology Design and Assessment. https://www.aceee.org/files/proceedings/2014/data/papers/9-702.pdf.

Tian, Zhen, and James A. Love. 2008. "A Field Study of Occupant Thermal Comfort and Thermal Environments with Radiant Slab Cooling." *Building and Environment* 43 (10): 1658–1670 (October).

Zeyghami, Mehdi, D. Yogi Goswami, and Elias Stefanakos. 2018. "A Review of Clear Sky Radiative Cooling Developments and Applications in Renewable Power Systems and Passive Building Cooling." *Solar Energy Materials and Solar Cells* 178 (May): 115–128.